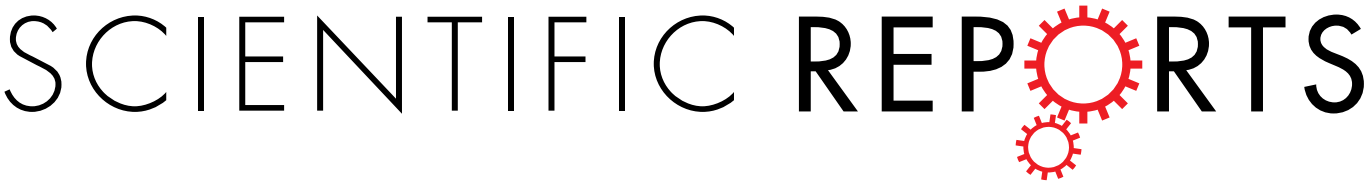

OPEN

$Ni(OH)_2$ nanosheets grown on porous hybrid g-C_3N_4/RGO network as high performance supercapacitor electrode

Received: 19 August 2016
Accepted: 23 January 2017
Published: 13 March 2017

Lei Li[1], Jia Qin[1], Huiting Bi[1], Shili Gai[1], Fei He[1], Peng Gao[1], Yunlu Dai[1], Xitian Zhang[2], Dan Yang[1] & Piaoping Yang[1]

A porous hybrid g-C_3N_4/RGO (CNRG) material has been fabricated through a facile hydrothermal process with the help of glucose molecules, and serves as an efficient immobilization substrate to support ultrathin $Ni(OH)_2$ nanosheets under an easy precipitation process. It was found that the g-C_3N_4 flakes can uniformly coat on both sides of the RGO, forming sandwich-type composites with a hierarchical structure. It is worth noting that the introduction of the g-C_3N_4 can effectively achieve the high dispersion and avoid the agglomeration of the nickel hydroxide, and significantly enhance the synthetically capacitive performance. Owning to this unique combination and structure, the CNRG/$Ni(OH)_2$ composite possesses large surface area with suitable pore size distribution, which can effectively accommodate the electrolyte ions migration and accelerate efficient electron transport. When used as electrode for supercapacitor, the hybrid material exhibits high supercapacitive performance, such as an admirable specific capacitance (1785 F/g at a current density of 2 A/g), desirable rate stability (retain 910 F/g at 20 A/g) and favorable cycling durability (maintaining 71.3% capacity after 5000 cycles at 3 A/g). Such desirable properties signify that the CNRG/$Ni(OH)_2$ composites can be a promising electrode material in the application of the supercapacitor.

Supercapacitors, as an essential part of applicable energy storage devices, have been widely employed in energy backup systems, electrical vehicles and portable electronic devices owing to their fast recharge ability, high power density, and environmental friendliness[1–3]. Generally, supercapacitors can be divided into two categories according to the energy storage mechanism: electrical double-layer capacitors (EDLCs) that store energy depending on the pure electrostatic charge accumulated at the interface of electrode/electrolyte, such as carbon materials with high specific area and excellent conductivity[4–8], and pseudocapacitors whose capacitance originates from reversible Faradaic reaction in the presence of electro-active species in the electrodes, including conducting polymers, transition metal oxides and hydroxides[9–11]. Pseudocapacitors exhibit much better capacitive behavior due to the fast and reversible faradic reaction compared to EDLCs[12–15]. However, during the long-term Faradaic processes, undesirable high rate stability and reversibility for these electrode materials have been critical drawbacks that hinder their practical applications[16–19]. Therefore, the constructing of new structured materials which integrated these two charge storage mechanisms, can take fully utilization of their synergistic mechanism and attain the goal of gaining eligible capacitor electrode[20–22].

Among all sorts of pseudo-active materials, nickel hydroxide is regarded as one of the most favorable material for capacitor electrode owning to its easy preparation, low cost and favorable theoretical specific capacitance[23–26]. Nevertheless, both poor electronic conductivity and large volumetric expansion of nickel hydroxide significantly restrict the electron transport and decelerate the redox reactions[27–29]. Moreover, it is subjected to aggregation upon cycling and unstable electrochemical interface between active material and electrolyte ascribed to an excessive surface energy[30,31]. To address this problem, one feasible and effective approach is to design novel hybrid

[1]Key Laboratory of Superlight Materials and Surface Technology, Ministry of Education, Harbin Engineering University, Harbin 150001, P. R. China. [2]Key Laboratory for Photonic and Electronic Bandgap Materials, Ministry of Education, School of Physics and Electronic Engineering, Harbin 150001, P.R. China. Correspondence and requests for materials should be addressed to P.G. (email: gaopeng@hrbeu.edu.cn) or X.Z. (email: xtzhangzhang@hotmail.com) or P.Y. (email: yangpiaoping@hrbeu.edu.cn)

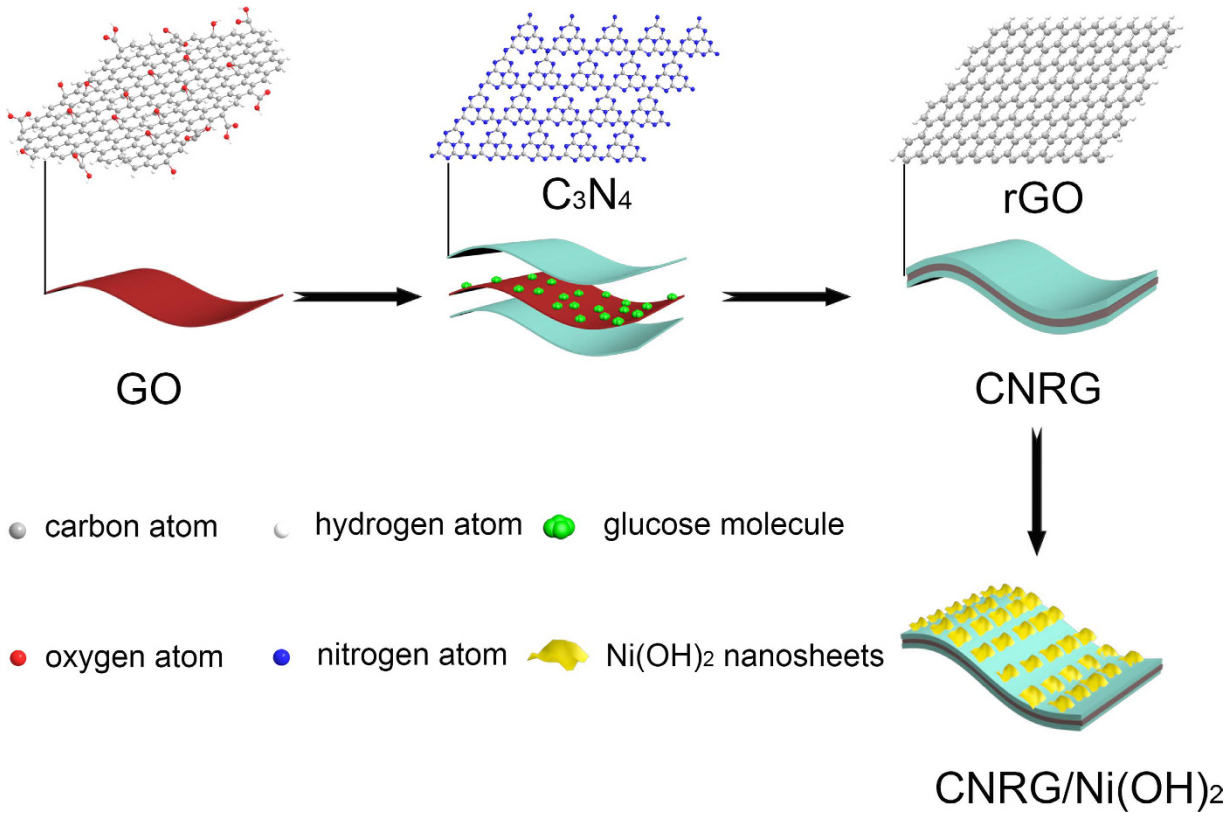

Figure 1. Schematic illustration for the preparation of CNRG/Ni(OH)$_2$ composite.

structure, which can optimize this pseudocapacitive materials to nano-size (nanoparticles or nanosheets) and confine them within a conductive carbonaceous matrix[32–35].

Graphene, a new member of carbonaceous material, can represent a desirable template in dispersing or wrapping active nanoparticles or nanosheets, avoiding aggregation and facilitating charge transportation benefiting from its high specific surface and extraordinary conductivity[36–38]. In particular, its two-dimensional sp^2-bonded structure can also provide great opportunity to increase the cycling stability of the as-synthesized material for the use of supercapacitor electrode[39]. With regard to the synthesis of graphene and Ni(OH)$_2$ hybrid material, the direct formation of nano-sized Ni(OH)$_2$ is inadvisable because of the weak bonding between nickel hydroxide and graphene leading to the falling of active nanoparticles or nanosheets away from the substrate[40]. To solve this problem, graphitic carbon nitride (g-C_3N_4) can be emerging as a suitable candidate combined with graphene for high loading nanocomposites[41]. For one thing, owning to the porous structure and high nitrogen content, g-C_3N_4 can offer more highly reactive region and binding defects to serve as an eligible template for crystals' nucleating and growing[42–44]. Additionally, g-C_3N_4 has lamellar structure and good lattice which can be well matched with graphene and hydroxide nanosheets[45,46]. For another thing, it was found that the combination of g-C_3N_4 with graphene can also enhance the electrochemical performance of g-C_3N_4[47]. Thus, it is of great significance to combine pseudocapacitive materials with carbon materials for high-performance electrode with the help of g-C_3N_4 nanosheets.

In this work, we construct a balanced and porous hierarchical CNRG/Ni(OH)$_2$ architecture, which can take advantage of the desirable conductivity of the graphene and trigger a synergistic effect from EDLCs and Ni(OH)$_2$ nanosheets. By utilizing g-C_3N_4 as template, abundant ultrathin Ni(OH)$_2$ nanosheets anchored on the carbon-based material firmly without agglomeration. Such unique structure significantly increases ionic accessibility and transmission, thus accelerating the rapid diffusion of electrolyte to access the active sites of Ni(OH)$_2$ nanosheets. When employed as electrode in supercapacitor, the CNRG/Ni(OH)$_2$ exhibits excellent electro-chemical performance in terms of specific capacitance, rate capability and cycling performance in comparison with pure Ni(OH)$_2$. On account of the remarkable properties of the as-prepared samples, we infer that this novel route towards the synthesis of electrode material will have practical application in the fields of conversion and energy storage systems.

Results and Discussion

Phase and Morphology Properties. Figure 1 illustrates the overall mechanism for the preparation of CNRG/Ni(OH)$_2$ *via* two main procedures. Firstly, the synthesis of CNRG was finished through a hydrothermal treatment with the aid of ammonia and glucose. In this process, oxygen-containing groups on GO sheets can be favorably bonded with glucose molecule via electrostatic and hydrogen conjugating interactions, which can not only serve as binder for the g-C_3N_4 but also reduce GO to RGO with the help of ammonia hydroxide.

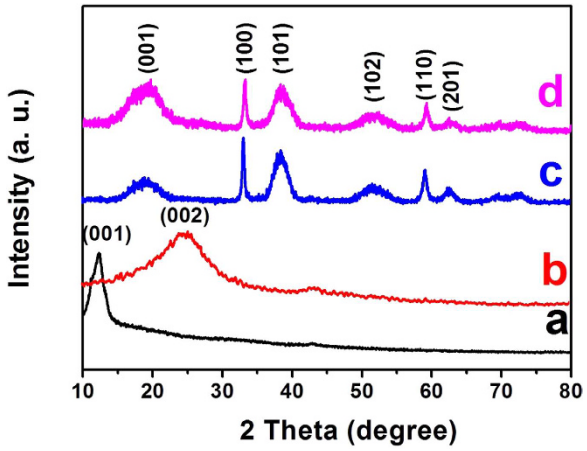

Figure 2. XRD patterns of GO (**a**), CNRG (**b**), pure $Ni(OH)_2$ (**c**) and CNRG/$Ni(OH)_2$ composite (**d**).

Afterwards, with the addition of $Ni(Ac)_2$, Ni^{2+}.ions can be bound onto the interior surface of g-C_3N_4, because plentiful nitrogen pots on the surface of g-C_3N_4 can generate strong chemical absorption with metal ions. Owning to this desirable effect, ultrathin $Ni(OH)_2$ nanosheets can uniformly deposit on the surface of C_3N_4 layer by a facile chemical precipitation method, triggering the formation of ternary g-C_3N_4/RGO/$Ni(OH)_2$ composites with increased hierarchy.

XRD patterns of as-synthesized GO, CNRG, pure $Ni(OH)_2$ and CNRG/$Ni(OH)_2$ are shown in Fig. 2. The sharp and intense diffraction peak of GO locates at about 11.6° corresponds to a layered structure, which is calculated to be a basal spacing of 0.76 nm (larger than that of previous graphite (0.34 nm)), indicating that oxygen groups are introduced into the graphitic layer and a well ordered structure of GO has emerged[22]. After the GO is reduced by glucose and coated with C_3N_4 nanosheets under hydrothermal process, we can see that the peak at 11.6° disappears and a broad peak at about 24.7° can be observed with interlayer spacing of 0.359 nm for CNRG, revealing that most of the oxygen functional groups of GO have been removed, which is beneficial to a further increasing in electrical conductivity[24,48]. For pure $Ni(OH)_2$ sample, it can be seen that all the peaks of the XRD patterns can be well indexed to the β-$Ni(OH)_2$ (JCPDS No. 14−0117). CNRG/$Ni(OH)_2$ has the similar diffraction pattern compared to that of pure $Ni(OH)_2$, implying that $Ni(OH)_2$ nanosheets can be well formed on the surface of C_3N_4. It is noteworthy that no characteristic peaks of GO or RGO can be found in the patterns of CNRG/$Ni(OH)_2$, demonstrating that high crystalline of $Ni(OH)_2$, which can be further confirmed by following characterization.

FESEM and TEM were employed to characterize the morphology and structure of CNRG. As displayed in Fig. 3A and B, the CNRG exhibits a silk-like morphology with a lot of winkles, which could prevent the sheets from stacking on each other. The rather smooth surface of CNRG confirms that the g-C_3N_4 have uniformly attached to GO substrate without any obvious agglomeration. The TEM images (Fig. 3C and D) of CNRG clearly show the uniformly dispersion of C_3N_4 nanosheets onto the surface of RGO. As presented in Fig. 3D, the resulting macroporosity of the C_3N_4 can serve as basal plane for high mass loading of $Ni(OH)_2$ and facilitate charge transport at high current density.

Figure 4A and B show the SEM images of the CNRG/$Ni(OH)_2$ composites, which exhibit a relatively rough surface compared with CNRG due to the adhesion of $Ni(OH)_2$ nanopetals. In addition, as displayed in Figure S1, the hybrid electrode can also maintain the morphology of the materials. From the TEM images of the CNRG/$Ni(OH)_2$ composites (Fig. 4C and D), we can clearly observe that the surface of CNRG is covered by ultrathin $Ni(OH)_2$ nanosheet densely. Owning to the strong interaction between g-C_3N_4 and $Ni(OH)_2$, layered $Ni(OH)_2$ nanosheets are firmly immobilized on surface of the porous CNRG and not peel off even after a long period of vigorous ultrasonic treatment for the preparation of TEM specimen. The selected area electron diffraction (SAED) pattern (inset of Fig. 4D) further shows the growth of $Ni(OH)_2$ nanocrystal on CNRG *in situ*. And the HRTEM image in Fig. 4E reveals that the calculated lattice spacing of the nanosheets is about 0.236 nm, which corresponds to the (101) plane of β-$Ni(OH)_2$. EDS mapping technique was conducted to determine the compositional and elemental distribution, and the results are shown in Fig. 4F. It can be clearly seen that the elements of C, Ni, and N are homogenously distributed, demonstrating the presence of C_3N_4 nanosheets and the uniform coating of $Ni(OH)_2$ nanosheets. Such unique ternary structure can provide more electrochemically active sites for $Ni(OH)_2$ to be exposed by electrolyte, meanwhile favor the ion transfer and diffusion, thus accelerating the surface redox reaction.

Raman spectra have been employed to clarify the degree of graphitization and the effect of nitrogen doping of RGO. Figure 5 presents the Raman spectrums for GO, CNRG and CNRG/$Ni(OH)_2$. As known, the intensity ratio of D band versus G band (I_D/I_G) is a significant parameter to the carbon hybridization state of materials and the degree of disorder[48,49]. An increased value (I_D/I_G) is obtained from GO (0.923) to those of CNRG (0.983) and CNRG/$Ni(OH)_2$ (0.981), implying the removal of the oxygen functional groups occurred on GO and more defects appear due to the heteroatomic doping of N from C_3N_4 nanosheets. Noteworthy, the G band of CNRG presents a downshift compared with that of GO, which is also caused by the nitrogen doping into the RGO framework[50,51].

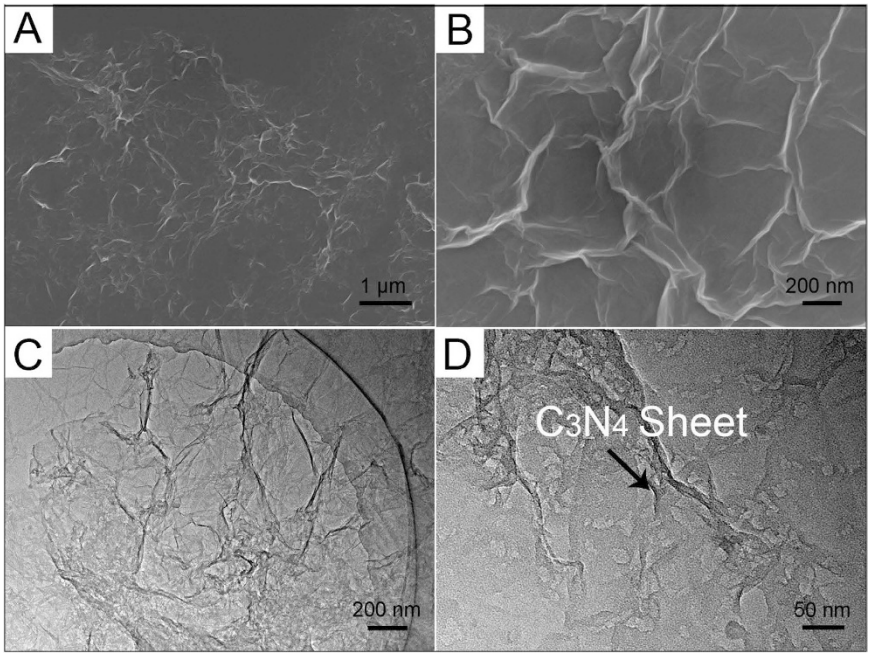

Figure 3. SEM (**A**,**B**) and TEM (**C**,**D**) images of CNRG composite.

The elemental composition and chemical valence for CNRG/$Ni(OH)_2$ composite were also elucidated by X-ray photoelectron spectra analysis. The survey spectrum (Fig. 6A) reveals the coexistence of C, Ni, O and N elements, which is consistent with the results of EDS mapping. And the high-resolution of C 1 s spectrum (Fig. 6B) can be fitted into a dominant peak and three relatively weak peaks, which are respectively assigned to sp^2 carbon (284.8 eV), C-O (286.1 eV), C-N (287.9 eV) and carbon in carbonyl (288.8 eV). This result suggests that during the hydrothermal process, the oxygen functional groups have been partially removed and the C_3N_4 nanosheets have been successfully introduced onto RGO[30,52]. Figure 6C depicts the high XPS resolution spectra of N 1 s on CNRG/$Ni(OH)_2$. Deconvolution of the core-level N 1 s shows three peaks at 398.7, 399.5 and 400.4 eV, corresponding to three different types of nitrogen states graphitic N, pyrrolic N and pyridinic N, which are consistent with the characteristic nitrogen species of the g-C_3N_4[44,47]. Previous reports have confirmed that the graphitic N can be conductive to improve the electrical conductivity of carbon-based electrode, and pyrrolic N and pyridinic N are able to create plenty of active sites and extrinsic defects, which are helpful for the fast transportation of the ions and increase capacitance of the composites[4,53]. In addition, the peaks located at 879.6 eV and 861.1 eV can be assigned to Ni $2p_{1/2}$ and Ni $2p_{3/2}$ satellites, respectively, with a spin-energy separation of 17.6 eV, which is characteristic of the $Ni(OH)_2$ phase[54,55].

It is well accepted that surface area and pore size are two crucial factors to determine the properties of electrode materials[56,57]. Figure 7A displays the nitrogen adsorption and desorption isotherms for CNRG/$Ni(OH)_2$ composite and pure $Ni(OH)_2$, and both of which exhibits a typical type IV with a H_3 hysteresis loop, suggesting the existence of mesopores of each sample. And the BET specific surface area of CNRG/$Ni(OH)_2$ is measured to be 250 m^2/g, which is markedly larger than that (63 m^2/g) of pure $Ni(OH)_2$, suggesting that positive effect of CNRG to avoid the aggregation of $Ni(OH)_2$, leading to higher exposure of the active sites. In comparison with pure $Ni(OH)_2$, the pore-size distribution curve of CNRG/$Ni(OH)_2$ shows narrow size distribution (4.1 nm) and a prominent volume increase in the range of 3–5 nm, which is favorable for electrochemical reactions[58,59]. Such unique mesoporous structure of CNRG/$Ni(OH)_2$ can not only guarantee a large electrode/electrolyte interface for electrostatic charge accumulation but also facilitate ion transport by shortening diffusion pathway, which is beneficial to the performance of the supercapacitor.

Electrochemical properties. To determine the potential application of CNRG/$Ni(OH)_2$ composite for high-performance supercapacitor, the cyclic voltammetry (CV) tests were carried out at various scan rates within the potential range from 0 to 0.5 V. As displayed in Fig. 8A, the potential of oxidation and reduction peaks shift towards more positive and negative direction with the increasing of the scan rates, which can be ascribed to the high electric polarization during the faradaic redox reaction at high scan rates. The redox peaks exhibit a symmetric shape, manifesting a high reversibility of this hybrid electrode materials. Moreover, the CV curves of CNRG/$Ni(OH)_2$ maintain a relatively similar shape at each scan rates, indicating that the electrode possesses a desirable rate stability owning to the good adsorption and facile ion diffusion properties[60]. To explore the capacitive characteristics of this composite, the charging-discharging tests were operated and the plots of voltage versus time at various densities were displayed in Fig. 8B. It can be observed that potential plateaus are presented in charge-discharge curves which match well with the peaks of the CV curves, implying the pseudo-capacitive behavior of CNRG/$Ni(OH)_2$. And the discharge time decreases monotonically with the increasing of current

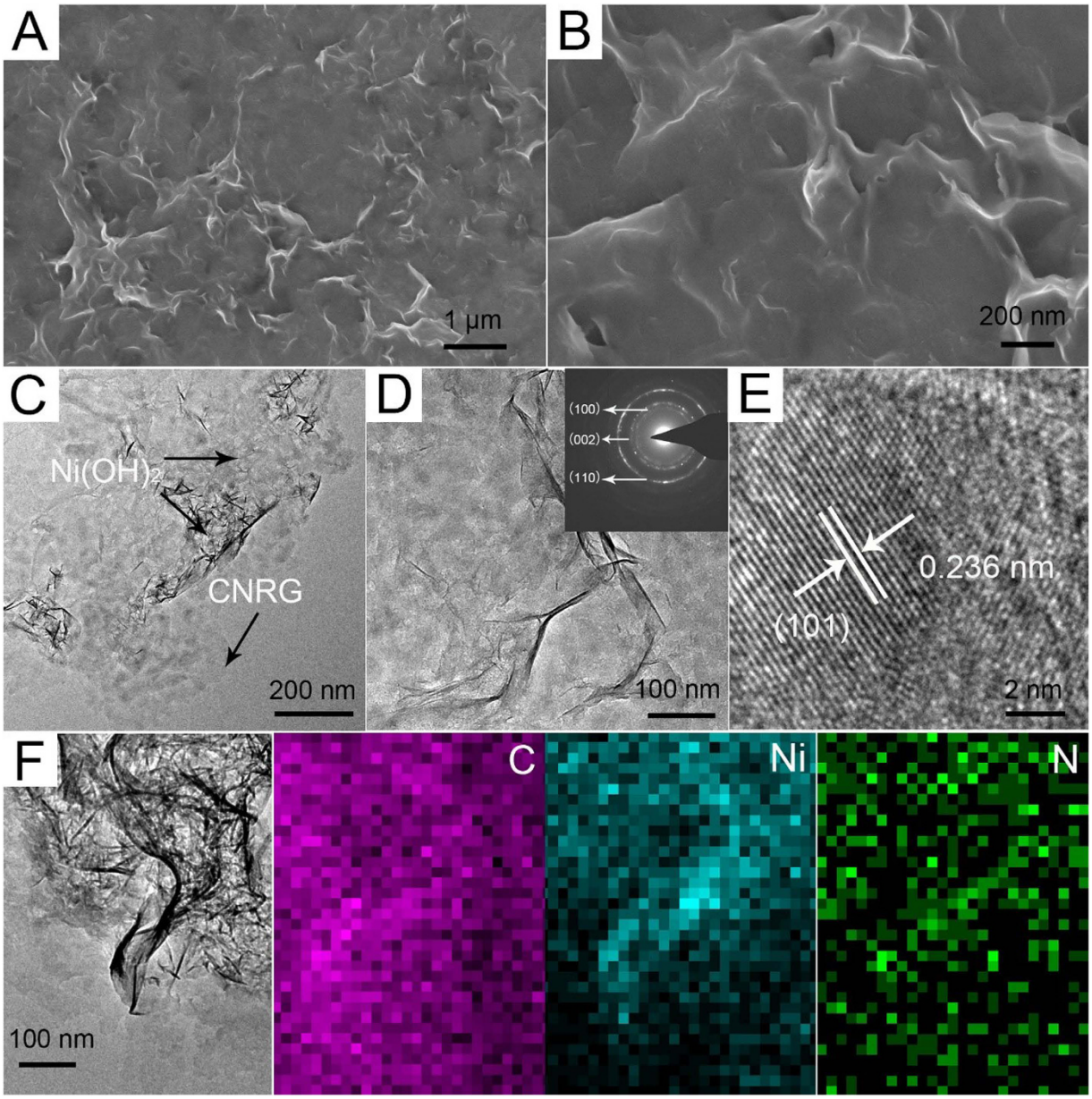

Figure 4. Low- and high-magnified SEM image (**A** and **B**), TEM images (**C** and **D**), SAED (inset of **D**), HRTEM image (**E**), HAADF-STEM image and elemental mapping images (**F**) of CNRG/$Ni(OH)_2$ composite.

densities, due to drastic redox reaction to satisfy fast potential change. And the value of specific capacitance for the composite has been calculated and the corresponding data is displayed in Fig. 9C for comparison.

To determine the positive role of CNRG on the improvement of supercapacitive properties for nickel hydroxide, the CV curves for CNRG/$Ni(OH)_2$ and pure $Ni(OH)_2$ at the scan rate of 5 mV/s are shown in Fig. 9A. It can be clearly seen that a couple of highly reversible redox peaks emerge in each curve during the cathodic and anodic sweeps, which can be ascribed to the redox reaction between $Ni(OH)_2$ and NiOOH in alkaline solution as follows: $Ni(OH)_2 + OH- \leftrightarrow NiOOH + H_2O + e^-$ [35,61]. Generally, the integral area of the CV curve is proportional to the value of capacitance[34]. And it can be figured out that the CV curve of CNRG/$Ni(OH)_2$ owns much larger area than that of pure $Ni(OH)_2$, suggesting that greatly enhanced specific capacitance has been obtained due to the introduction of CNRG. And the charge-discharge tests have been also conducted to verify better electrochemical performance of CNRG/$Ni(OH)_2$. In Fig. 9B, the curve of CNRG/$Ni(OH)_2$ composite presents a much longer discharge time than that of pure $Ni(OH)_2$, which further confirm the much favorable specific capacitance of CNRG/$Ni(OH)_2$. Figure 9C exhibits the rate performance of as-prepared samples according to the capacitive value versus different current densities. Encouragingly, CNRG/$Ni(OH)_2$ composite possesses much higher capacitive performance than that of pure $Ni(OH)_2$ at each current density. And we have included the total mass of $Ni(OH)_2$ and CNRG to determine specific capacitance of the CNRG/$Ni(OH)_2$ composite. Based on the Equation 1, the specific capacitance for CNRG/$Ni(OH)_2$ at 2 A/g can be calculated as 1785 F/g, and retain at 910 F/g with the current

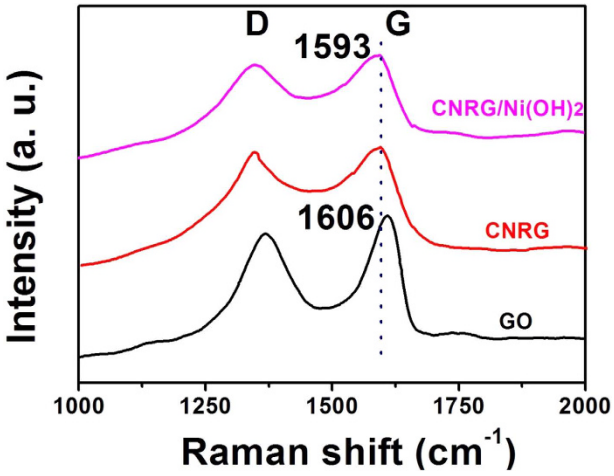

Figure 5. Raman spectra of GO, CNRG and CNRG/Ni(OH)$_2$ composite.

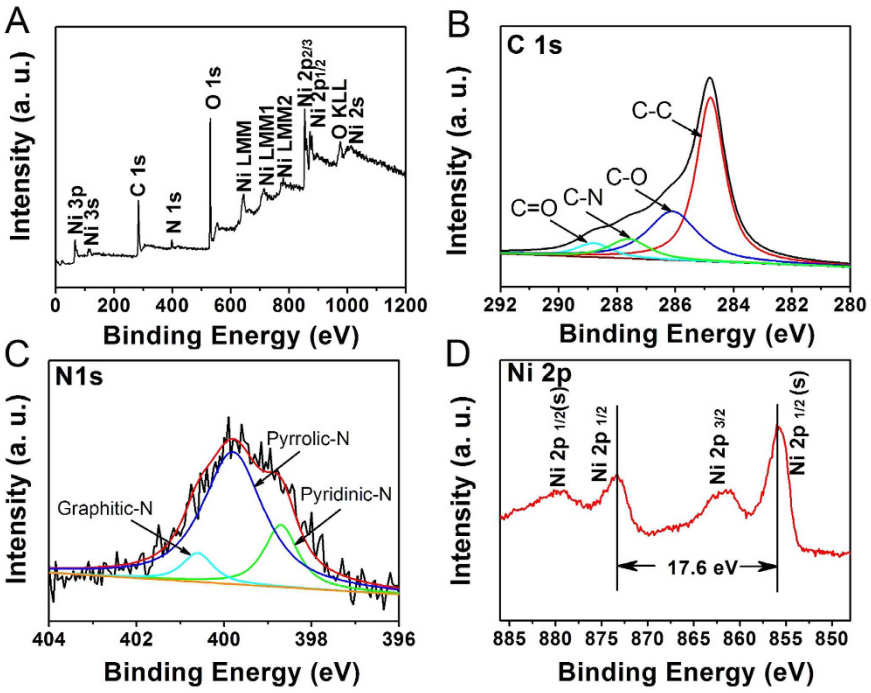

Figure 6. XPS spectra of CNRG/Ni(OH)$_2$ composite: survey spectrum (**A**), C 1 s (**B**), N 1 s (**C**) and Ni 2p (**D**).

density up to 20 A/g, demonstrating desirable rate capability, which is an important factor for the electrode materials to provide high power density[8,13]. Whereas at the same density, pure Ni(OH)$_2$ exhibits comparatively poor specific capacitance of 1106 F/g and 450 F/g with an unsatisfied retention of 41%. The reason for the admirable specific capacitance and rate performance of this hybrid electrode is the interactive effect between the CNRG and Ni(OH)$_2$. On one hand, ultra-thin Ni(OH)$_2$ nanosheets can offer amount of active sites for faradaic reaction and account for dominant electrochemical capacitance; on the other hand, the CNRG can avoid the agglomeration of Ni(OH)$_2$ nanosheets and enhance ion transfer.

The remarkably electrochemical performance for the CNRG/Ni(OH)$_2$ hybrid electrode was further assessed through the electrochemical impedance spectroscopy measurements within the frequency range from 0.1 Hz to 100 kHz. As shown in Fig. 9D, the impedance plots of both samples consists of a semicircle in the high-frequency region and a relative straight line in the low-frequency region. As generally accepted to us, the semicircle diameter of EIS curve represents the electrochemical reaction impedance of the electrode, and the straight line is associated with the ion-diffusion resistance[20,62]. As presented in inset of Fig. 9D, the CNRG/Ni(OH)$_2$ displays a much smaller semicircle over the high frequency range, and a more upright line than those of pure Ni(OH)$_2$, implying this hybrid composite possesses faster ion diffusion process and lower charge transfer resistance during

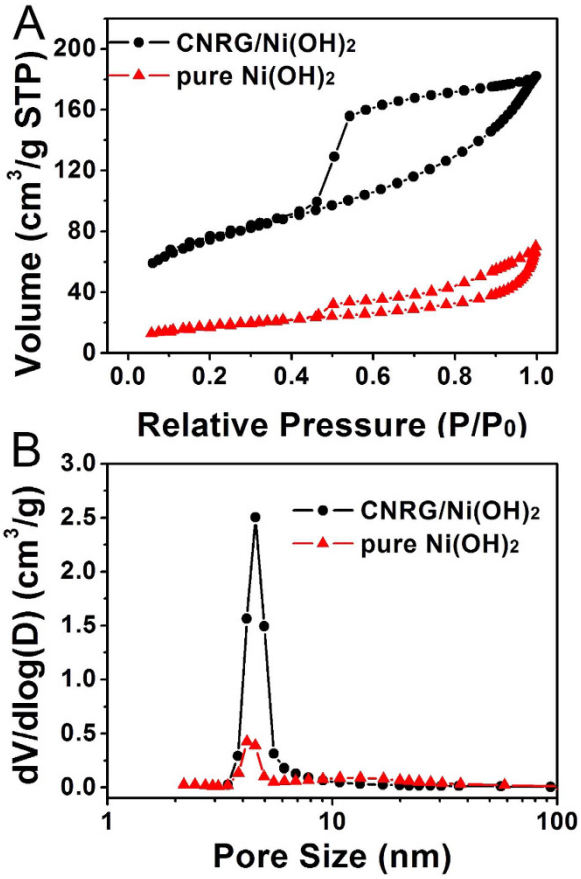

Figure 7. N_2 adsorption/desorption isotherms (**A**) and the corresponding pore size distributions (**B**) of pure $Ni(OH)_2$ and CNRG/$Ni(OH)_2$ composite.

the faradic reaction[63]. It can be concluded that the high electronic conductivity of the CNRG/$Ni(OH)_2$ can be ascribed to the unique structure of CNRG with large surface area and porous feature, which can make $Ni(OH)_2$ nanosheets keep highly interconnected with each other to facilitate the electron transport.

As cycling performance is a decisive parameter for applications of supercapacitor electrode, the stability test of CNRG/$Ni(OH)_2$ composite was conducted *via* charge-discharge technique at 3 A/g for 5000 cycles. As shown in Fig. 10, for the cycling performance, during the initial cycles, the capacitance of CNRG/$Ni(OH)_2$ presents a slight increase, which can be ascribed to electrode activation ascribed to the increasing of available active sites and the gradual diffusion of the trapped ions during activation process. Notably, the capacitance of CNRG/$Ni(OH)_2$ composite retains 71.3% after 5000 charge-discharge cycles, suggesting that this electrode exhibits much admirable cycling electrochemical durability under identical test conditions. This result indicates that the synergistic combination between CNRG and $Ni(OH)_2$ can effectively prevent aggregation of the active materials and accommodate the volume change during cycling process.

Above all, this work reports a novel and facile design for the fabrication of the g-C_3N_4/RGO (CNGR) mesoporous hybrid framework to serve as substrate for the formation of the $Ni(OH)_2$ nanosheets. Because of the localized highly reactive region and binding defects of the g-C_3N_4, the CNRG can offer a large number of anchoring sites and prevent the agglomeration of the $Ni(OH)_2$. Benefiting from the rational structural features which can effectively favor the ion transfer and diffusion, this composite exhibits excellent specific capacitance, desirable rate capability and cycling durability when served as electrode. These results demonstrate that the CNRG/$Ni(OH)_2$ material with unique structure can be a promising electrode material for supercapacitor application.

Methods

Synthesis of g-C_3N_4/RGO (CNRG) composite. Graphene oxide (GO) was synthesized based on a modified Hummers method through the oxidation of natural graphite powder[22]. For the preparation of g-C_3N_4, melamine as precursor was calcinated for 3 h in the air atmosphere under 550 °C with a rate ramp of 4 °C min^{-1}. Then a certain amount bulk g-C_3N_4 was decentralized uniformly in 30 mL of distilled water with ultra-sonication for over 18 h. For the synthesis of CNRG, 25 mL of 2.8 mg mL^{-1} GO solution was dispersed in the solution of g-C_3N_4, added with 0.5 g glucose and 1 mL ammonia, and then moved into a high pressure autoclave to keep for 12 hours at 180 °C. When the reaction was cooled to room temperature naturally, the obtained precipitates were centrifuged and washed with deionized water for several times.

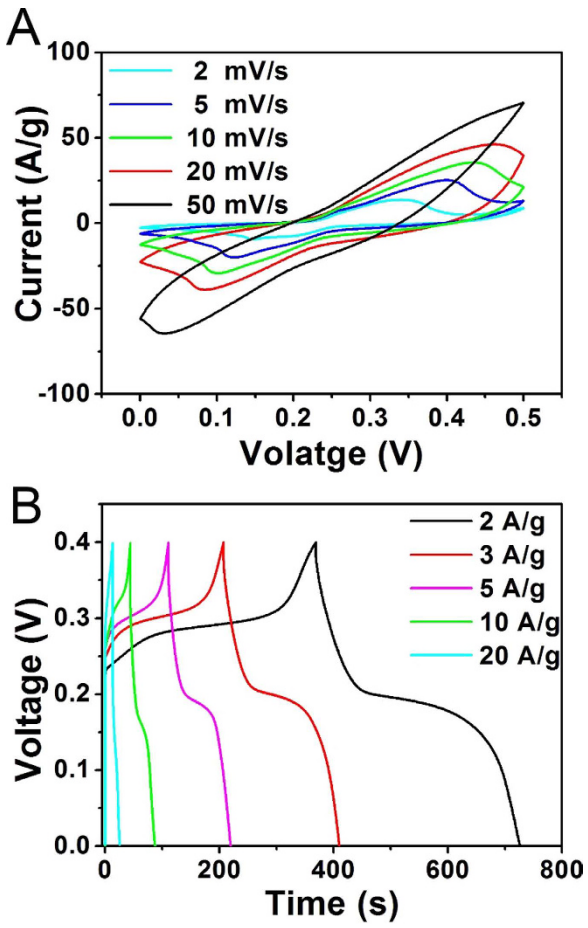

Figure 8. Cyclic voltammograms (**A**) of CNRG/Ni(OH)$_2$ electrodes measured at scan rates from 2–50 mV/s, and charge-discharge curves (**B**) of CNRG/Ni(OH)$_2$ measured at various discharge current.

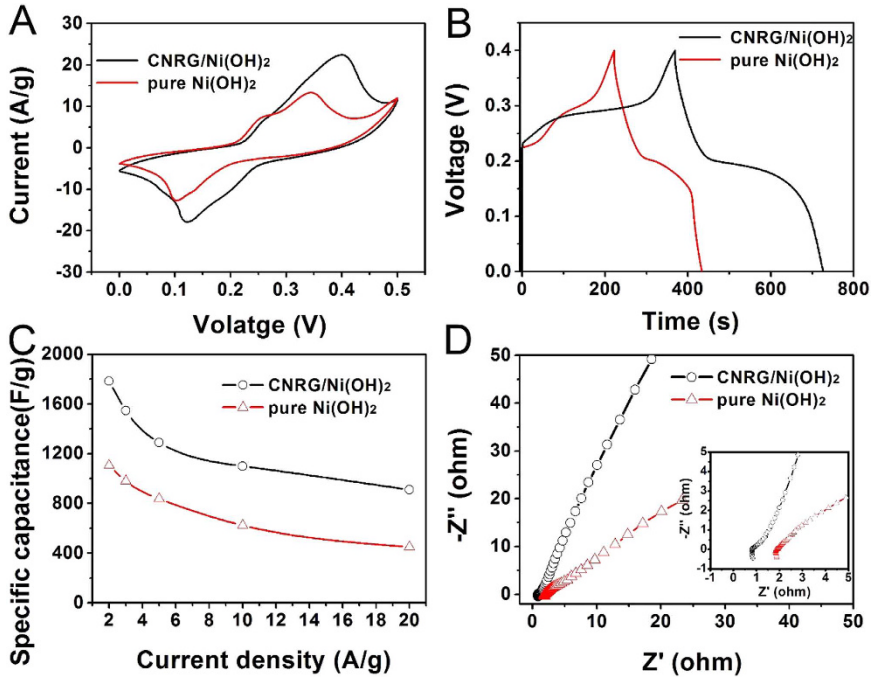

Figure 9. Cyclic voltammograms (CVs) curves (**A**), galvanostatic (GV) charge-discharge curves (**B**), current density dependence of the specific capacitance (**C**), and Nyquist plots of the EIS for CNRG and CNRG/Ni(OH)$_2$ composite (**D**).

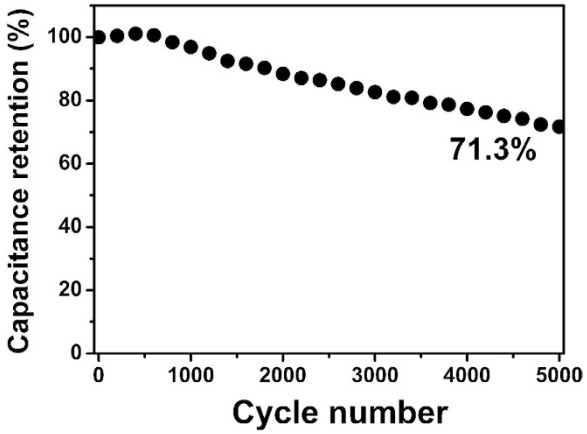

Figure 10. Cycling performance of CNRG/Ni(OH)$_2$ composite measured at a current density of 3 A/g.

Synthesis of CNRG/Ni(OH)$_2$ composites. The above products with the addition of 4 mL ammonia were dissolved in 170 mL of solvent (water/ethanol = 1/1, *V/V*) by hyperacoustic treatment. And then the solution was transferred into a three-necked flask under continuous stirring. After 20 min, 2.5 mmol of Ni(Ac)$_2$ was gradually added into the above homogeneous solution and refluxed at 85 °C in an oil bath for 6 h. The products were collected by centrifugation and washed with distilled water and ethanol three times respectively. Finally, the precipitation was dried in a vacuum oven at 60 °C for 12 h. Pure Ni(OH)$_2$ was prepared in the same method in the absence of CNRG composites as a comparison.

Fabrication of electrode and electrochemical measurement. The electrochemical properties of CNRG/Ni(OH)$_2$ are evaluated by previous method. The conventional three-electrode cell was consisted of the counter electrode (Pt foil of $1 \times 1\,cm^2$), the reference electrode (a Ag/AgCl electrode) and working electrode (Ni foam coated with active material), respectively. The weight of the active materials is about 3.5 mg. All measurements were conducted at room temperature and the electrolyte is the 6 M KOH aqueous solution. According to galvanostatic charge-discharge curves, the specific capacitance values of the electrode can be calculated by the following equation: $C = I\Delta t/m\Delta V$ (1), where I is the response current density, Δt is the discharge time, m is the mass of the active materials on single electrode, ΔV is the potential range during the charge-discharge measurement.

Characterization. Crystalline structure, the morphology, and chemical composition of the samples were investigated by powder X-ray diffraction (XRD) (Rigaku D/max TTR-III diffractometer with graphite monochromatized Cu Kα radiation ($\lambda = 0.15405$ nm)), scanning electron microscope (SEM, JSM-6480A), transmission electron microscopy (TEM, FEI Tecnai G2 S-Twin), high-resolution transmission electron microscopy (HRTEM), and the X-ray photoelectron spectra XPS (VG ESCALAB MK II electron energy spectrometer using Mg KR (1253.6 eV) as the X-ray excitation source). Raman spectra were conducted on a confocal laser micro-Raman spectrometer (LABRAM-HR, JY Co.), and N_2 adsorption/desorption isotherms were measured from Micromeritics ASAP Tristar II 3020 apparatus. The electrochemical properties were carried out by a CHI 666D electrochemical workstation. All the tests were carried out at room temperature.

References

1. Yuan, C. *et al.* Growth of ultrathin mesoporous Co_3O_4 nanosheet arrays on Ni foam for high performance electrochemical capacitors. *Energy Environ. Sci.* **5,** 7883–7887 (2012).
2. Peng, L. L. *et al.* Ultrathin Two-Dimensional MnO_2/Graphene Hybrid Nanostructures for High Performance, Flexible Planar Supercapacitors. *Nano Lett.* **13,** 2151–2157 (2013).
3. Xu, S. *et al.* Nanofoaming to Boost the Electrochemical Performance of Ni@Ni(OH)$_{(2)}$ Nanowires for Ultrahigh Volumetric Supercapacitors. *ACS Appl. Mater. Interfaces* **8,** 27868–27876 (2016).
4. Yang, Z. *et al.* Recent Advancement of Nanostructured Carbon for Energy Applications. *Chem. Rev.* **115,** 5159–5223 (2015).
5. Zhou, Y., Candelari, S. L., Liu, Q., Uchaker, E. & Cao, G. Porous carbon with high capacitance and graphitization through controlled addition and removal of sulfur-containing compounds. *Nano Energy* **12,** 567–577 (2015).
6. Shao, Y. *et al.* Graphene-based materials for flexible supercapacitors. *Chem. Soc. Rev.* **44,** 3639–3665 (2015).
7. Wang, X. & Shi, G. Flexible graphene devices related to energy conversion and storage. *Energy Environ. Sci.* **8,** 790–823 (2015).
8. Xiong, P. *et al.* Ternary manganese ferrite/graphene/polyaniline nanostructure with enhanced electrochemical capacitance performance. *J. Power Sources* **266,** 384–392 (2014).
9. Wu, X. *et al.* Template synthesis of hollow fusiform RuO_2 center dot xH_2O nanostructure and its supercapacitor performance. *J. Mater. Chem. A* **1,** 469–472 (2013).
10. Zhao, C. *et al.* One-step hydrothermal preparation of TiO_2/RGO/Ni(OH)$_{(2)}$/NF electrode with high performance for supercapacitors. *Electrochim. Acta* **218,** 216–227, (2016).
11. Lee, D. U. *et al.* Self-Assembled NiO/Ni(OH)$_{(2)}$ Nanoflakes as Active Material for High-Power and High-Energy Hybrid Rechargeable Battery. *Nano Lett.* **16,** 1794–1802, (2016)
12. Su, X., Gao, C., Cheng, M. & Wang, R. Controllable synthesis of Ni(OH)$_{(2)}$/Co(OH)$_{(2)}$ hollow nanohexagons wrapped in reduced graphene oxide for supercapacitors. *RSC Adv.* **6,** 97172–97179, (2016)

13. Sun, W., Rui, X., Ulaganathan, M., Madhavi, S. & Yan, Q. Few-layered $Ni(OH)_2$ nanosheets for high-performance supercapacitors. *J. Power Sources* **295,** 323–328 (2015).
14. Qian, Y. *et al.* Efficient synthesis of hierarchical NiO nanosheets for high-performance flexible all-solid-state supercapacitors. *J. Mater. Chem. A* **2,** 10917–10922 (2014).
15. Gong, X. F., Cheng, J. P., Liu, F., Zhang, L. & Zhang, X. B. Nickel-Cobalt hydroxide microspheres electrodepositioned on nickel cobaltite nanowires grown on Ni foam for high-performance pseudocapacitors. *J. Power Sources* **267,** 610–616 (2014).
16. Chen, Y. L. *et al.* Nickel oxide nanoflake-based bifunctional glass electrodes with superior cyclic stability for energy storage and electrochromic applications. *J. Mater. Chem. A* **3,** 20614–20618 (2015).
17. Jo, C. *et al.* Block-Copolymer-Assisted One-Pot Synthesis of Ordered Mesoporous WO_3-x/Carbon Nanocomposites as High-Rate-Performance Electrodes for Pseudocapacitors. *Adv. Funct. Mater.* **23,** 3747–3754 (2013).
18. Choi, B. G., Huh, Y. S., Hong, W. H., Kim, H. J. & Park, H. S. Electrochemical assembly of MnO_2 on ionic liquid-graphene films into a hierarchical structure for high rate capability and long cycle stability of pseudocapacitors. *Nanoscale* **4,** 5394–5400 (2012).
19. Jiang, J. A. *et al.* Large-Scale Uniform alpha-$Co(OH)_{(2)}$ Long Nanowire Arrays Grown on Graphite as Pseudocapacitor Electrodes. *ACS Appl. Mater. Interfaces* **3,** 99–103 (2011).
20. Li, Z. *et al.* Rapid synthesis of graphene/cobalt hydroxide composite with enhanced electrochemical performance for supercapacitors. *J. Power Sources* **245,** 224–231 (2014).
21. Li, M., Ma, K. Y., Cheng, J. P., Lv, D. & Zhang, X. B. Nickel–cobalt hydroxide nanoflakes conformal coating on carbon nanotubes as a supercapacitive material with high-rate capability. *J. Power Sources* **286,** 438–444 (2015).
22. Xu, J. *et al.* A sandwich-type three-dimensional layered double hydroxide nanosheet array/graphene composite: fabrication and high supercapacitor performance. *J. Mater. Chem. A* **2,** 1022–1031 (2014).
23. Salunkhe, R. R. *et al.* Large-scale synthesis of coaxial carbon nanotube/$Ni(OH)_2$ composites for asymmetric supercapacitor application. *Nano Energy* **11,** 211–218 (2015).
24. Min, S. *et al.* Synthesis of $Ni(OH)_2$/RGO pseudocomposite on nickel foam for supercapacitors with superior performance. *J. Mater. Chem. A* **3,** 3641–3650 (2015).
25. Pavul Raj, R., Mohan, S. & Jha, S. K. Controlled reverse pulse electrosynthesized spike-piece-structured Ni/Ni(OH)2 interlayer nanoplates for electrochemical pseudocapacitor applications. *Chem Commun. (Camb)* **52,** 1930–3 (2016).
26. Zhu, X., Zhang, P., Xu, S., Yan, X. & Xue, Q. Free-standing three-dimensional graphene/manganese oxide hybrids as binder-free electrode materials for energy storage applications. *ACS Appl. Mater. Interfaces* **6,** 11665–74 (2014).
27. Du, H., Wang, Y., Yuan, H. & Jiao, L. Facile Synthesis and High Capacitive Performance of 3D Hierarchical $Ni(OH)_2$ Microspheres. *Electrochim. Acta* **196,** 84–91 (2016).
28. Li, J., Zhao, W., Huang, F., Manivannan, A. & Wu, N. Single-crystalline $Ni(OH)_2$ and NiO nanoplatelet arrays as supercapacitor electrodes. *Nanoscale* **3,** 5103 (2011).
29. Liu, Y., Wang, R. & Yan, X. Synergistic Effect between Ultra-Small Nickel Hydroxide Nanoparticles and Reduced Graphene Oxide sheets for the Application in High-Performance Asymmetric Supercapacitor. *Sci. Rep.* **5,** 11095 (2015).
30. Zhang, H. *et al.* One-step electrophoretic deposition of reduced graphene oxide and $Ni(OH)_2$ composite films for controlled syntheses supercapacitor electrodes. *J. Phys. Chem. B* **117,** 1616–27 (2013).
31. Li, L. *et al.* A one-step, cost-effective green method to *in situ* fabricate $Ni(OH)_2$hexagonal platelets on Ni foam as binder-free supercapacitor electrode materials. *J. Mater. Chem. A* **3,** 1953–1960 (2015).
32. Alhebshi, N. A., Rakhi, R. B. & Alshareef, H. N. Conformal coating of $Ni(OH)_2$ nanoflakes on carbon fibers by chemical bath deposition for efficient supercapacitor electrodes. *J. Mater. Chem. A* **1,** 14897 (2013).
33. Xia, X. *et al.* One-pot synthesis and electrochemical properties of nitrogen-doped graphene decorated with M(OH)x (M = FeO, Ni, Co) nanoparticles. *Electrochim. Acta* **113,** 117–126 (2013).
34. Ma, X. *et al.* Ultrathin beta-$Ni(OH)_2$ nanoplates vertically grown on nickel-coated carbon nanotubes as high-performance pseudocapacitor electrode materials. *ACS Appl. Mater. Interfaces* **7,** 974–9 (2015).
35. Tang, Y. *et al.* Highly Oxidized Graphene Anchored $Ni(OH)_2$ Nanoflakes as Pseudocapacitor Materials for Ultrahigh Loading Electrode with High Areal Specific Capacitance. *J. Phys. Chem. C* **118,** 24866–24876 (2014).
36. Li, F., Jiang, X., Zhao, J. & Zhang, S. Graphene oxide: A promising nanomaterial for energy and environmental applications. *Nano Energy* **16,** 488–515 (2015).
37. Han, S., Wu, D., Li, S., Zhang, F. & Feng, X. Porous Graphene Materials for Advanced Electrochemical Energy Storage and Conversion Devices. *Adv. Mater.* **26,** 849–864 (2014).
38. Chen, S., Zhu, J. W., Qiu, L., Li, D. & Wang, X. Facile Fabrication of Nanoparticles Confined in Graphene Films and Their Electrochemical Properties. *Chem.-Eur. J.* **19,** 7631–7636 (2013).
39. Liu, W. *et al.* Ionic liquid-assisted grown of beta-nickel hydroxide nanowires on reduced graphene oxide for high-performance supercapacitors. *Electrochim. Acta* **143,** 135–142 (2014).
40. Chang, H. *et al.* Low-temperature solution-processable $Ni(OH)_2$ ultrathin nanosheet/N-graphene nanohybrids for high-performance supercapacitor electrodes. *Nanoscale* **6,** 5960–6 (2014).
41. Hou, Y. *et al.* N-doped graphene/porous g-C_3N_4 nanosheets supported layered-MoS_2 hybrid as robust anode materials for lithium-ion batteries. *Nano Energy* **8,** 157–164 (2014).
42. Xu, L. *et al.* Reactable ionic liquid assisted solvothermal synthesis of graphite-like C_3N_4 hybridized alpha-Fe_2O_3 hollow microspheres with enhanced supercapacitive performance. *J. Power Sources* **245,** 866–874 (2014).
43. Shi, L. *et al.* Flower-like $Ni(OH)_2$ hybridized g-C_3N_4 for high-performance supercapacitor electrode material. *Mater. Lett.* **145,** 150–153 (2015).
44. Zhang, L. *et al.* Enhanced supercapacitive performance of graphite-like C_3N_4 assembled with NiAl-layered double hydroxide. *Electrochim. Acta* **186,** 292–301 (2015).
45. Duan, X. *et al.* Nitrogen-doped graphene for generation and evolution of reactive radicals by metal-free catalysis. *ACS Appl. Mater. Interfaces* 7, 4169–78 (2015).
46. Duan, J., Chen, S., Jaroniec, M. & Qiao, S. Z. Porous C_3N_4 Nanolayers@N-Graphene Films as Catalyst Electrodes for Highly Efficient Hydrogen Evolution. *Acs Nano* **9,** 931–940 (2015).
47. Chen, Q., Zhao, Y., Huang, X., Chen, N. & Qu, L. Three-dimensional graphitic carbon nitride functionalized graphene-based high-performance supercapacitors. *J. Mater. Chem. A* **3,** 6761–6766 (2015).
48. Fu, Y., Zhu, J., Hu, C., Wu, X. & Wang, X. Covalently coupled hybrid of graphitic carbon nitride with reduced graphene oxide as a superior performance lithium-ion battery anode. *Nanoscale* **6,** 12555–64 (2014).
49. Zhu, X., Zhong, Y., Zhai, H., Yan, Z. & Li, D. Nanoflake nickel hydroxide and reduced graphene oxide composite as anode materials for high capacity lithium ion batteries. *Electrochim. Acta* **132,** 364–369 (2014).
50. Wang, X. *et al.* Atomistic origins of high rate capability and capacity of N-doped graphene for lithium storage. *Nano Lett.* **14,** 1164–71 (2014).
51. Deng, D. *et al.* Toward N-Doped Graphene via Solvothermal Synthesis. *Chem. Mater.* **23,** 1188–1193 (2011).
52. You, B., Wang, L., Yao, L. & Yang, J. Three dimensional N-doped graphene-CNT networks for supercapacitor. *Chem. Commun.* **49,** 5016–5018 (2013).
53. John, A. R. & Arumugam, P. Open ended nitrogen-doped carbon nanotubes for the electrochemical storage of energy in a supercapacitor electrode. *J. Power Sources* **277,** 387–392 (2015).

54. Zhang, F. *et al.* A nickel hydroxide-coated 3D porous graphene hollow sphere framework as a high performance electrode material for supercapacitors. *Phys. Chem. Chem. Phys.* **16,** 4186–92 (2014).
55. Yan, H. *et al*. Graphene homogeneously anchored with $Ni(OH)_2$ nanoparticles as advanced supercapacitor electrodes. *CrystEngComm* **15,** 10007 (2013).
56. Yang, W. *et al.* Solvothermal one-step synthesis of Ni-Al layered double hydroxide/carbon nanotube/reduced graphene oxide sheet ternary nanocomposite with ultrahigh capacitance for supercapacitors. *ACS Appl. Mater. Interfaces* **5,** 5443–54 (2013).
57. Candelaria, S. L. *et al.* Nanostructured carbon for energy storage and conversion. *Nano Energy* **1,** 195–220 (2012).
58. Peng, H. *et al*. Facile Synthesis of Poly(p-phenylenediamine)-Derived Three-Dimensional Porous Nitrogen-Doped Carbon Networks for High Performance Supercapacitors. *J. Phys. Chem. C* **118,** 29507–29516 (2014).
59. Zhao, Y., Meng, Y. & Jiang, P. Carbon@MnO_2 core–shell nanospheres for flexible high-performance supercapacitor electrode materials. *J.Power Sources* **259,** 219–226 (2014).
60. Peng, S. J., Li, L. L., Wu, H. B., Madhavi, S. & Lou, X. W. Controlled Growth of $NiMoO_4$ Nanosheet and Nanorod Arrays on Various Conductive Substrates as Advanced Electrodes for Asymmetric Supercapacitors. *Adv. Energy Mater.* **5** (2015).
61. Yang, Y., Cheng, D., Chen, S., Guan, Y. & Xiong, J. Construction of Hierarchical $NiCo_2S_4$@$Ni(OH)_2$ Core-Shell Hybrid Nanosheet Arrays on Ni Foam for High-Performance Aqueous Hybrid Supercapacitors. *Electrochim. Acta* **193,** 116–127 (2016).
62. Chen, J., Wang, X., Wang, J. & Lee, P. S. Sulfidation of NiMn-Layered Double Hydroxides/Graphene Oxide Composites toward Supercapacitor Electrodes with Enhanced Performance. *Adv. Energy Mater.* **6,** 1501745–1501752 (2016).
63. Nagaraju, G., Raju, G. S., Ko, Y. H. & Yu, J. S. Hierarchical Ni-Co layered double hydroxide nanosheets entrapped on conductive textile fibers: a cost-effective and flexible electrode for high-performance pseudocapacitors. *Nanoscale* **8,** 812–25 (2016).

Acknowledgements

Financial supports from the National Natural Science Foundation of China (NSFC 21401032, 51472058, and 51502050), China Postdoctoral Science Foundation (2014M560248, 2015T80321), Natural Science Foundation of Heilongjiang Province (B201403), Outstanding Youth Foundation of Heilongjiang Province (JC2015003), Heilongjiang Postdoctoral Fund (LBH-Z14052, LBH-TZ0607) and the Fundamental Research funds for the Central Universities are greatly acknowledged.

Author Contributions

L.L. designed the strategy for preparing the samples, carried out experiment and wrote the manuscript. X.Z., P.G. and P.Y. provided the research approach and scientific discussion at various stages. J.Q., H.B. and L.L. performed the electrochemical measurements. S.G., F.H., Y.D. and D.Y. collected data of phase and morphology. All authors reviewed the manuscript.

Additional Information

Supplementary information accompanies this paper at http://www.nature.com/srep

Competing financial interests: The authors declare no competing financial interests.

How to cite this article: Li, L. *et al.* $Ni(OH)_2$ nanosheets grown on porous hybrid g-C_3N_4/RGO network as high performance supercapacitor electrode. *Sci. Rep.* **7**, 43413; doi: 10.1038/srep43413 (2017).

Publisher's note: Springer Nature remains neutral with regard to jurisdictional claims in published maps and institutional affiliations.